Correlation between radius and asphericity in surfaces fitted by conics

Alfonso Pérez-Escudero, Carlos Dorronsoro, and Susana Marcos*

Instituto de Óptica, Consejo Superior de Investigaciones Científicas, Madrid, Spain
**Corresponding author: susana@io.cfmac.csic.es*

Received December 23, 2009; revised March 20, 2010; accepted May 3, 2010;
posted May 3, 2010 (Doc. ID 121769); published June 2, 2010

The optical surfaces of the eye are often described in terms of their radius and asphericity. The variations caused by experimental noise in repeated measurements of radius and asphericity of the same surface are strongly correlated. We show this correlation in experimental corneal elevation data from videokeratoscopy and Scheimpflug topography, in non-contact profilometry data of artificial lenses, and in simulations. The effect is a characteristic of the fits to conic curves, and not restricted to any experimental device or fitting procedure. A separate analysis of radius and asphericity may estimate incorrectly the statistical significance of the changes in the ocular surfaces. We propose a MANOVA-based statistical analysis that increases sensitivity by a factor of 4.

OCIS codes: 330.4875, 330.7325.

1. INTRODUCTION

Ocular surfaces are typically described by surfaces whose profiles are conic sections. The general equation of a conic curve is

$$x^2 = 2Ry - (1+Q)y^2, \tag{1}$$

where R and Q are the apical radius and asphericity, respectively. The apical direction is along the y-axis. Any conic is described in terms of these two parameters: the radius R representing the radius of curvature at the apex of the conic section and the asphericity Q representing the deviation of the conic from a circle. Conic curves are classified in circles ($Q=0$), hyperbolas ($Q<-1$), parabolas ($Q=-1$), and ellipses ($Q>-1$).

Radius and asphericity have been widely used to characterize the geometry of the cornea [1–4] and the crystalline lens. For example, they have been used in descriptions of the optical biometry of different populations, such as myopes and hyperopes (see Llorente *et al.* [5] and references therein), evaluation of diurnal changes in corneal topography [6], analysis of the changes in anterior and posterior corneal geometries with aging [7], evaluation of the geometrical changes induced by corneal refractive surgery [8,9], or design of custom-guided ablation algorithms aiming at controlling anterior corneal asphericity [10]. They have also been used to describe the geometry of the crystalline lens *in vitro* [11] and *in vivo* as a function of age [12], and *in vivo* as a function of accommodation [12–14].

Contact and intraocular lenses have evolved to aspheric designs, allowing the manipulation of the spherical aberration that they induce. In contact lenses, aspheric monofocal designs may provide a better optical quality [15], and also may modify the depth of focus in multifocal designs [16]. In intraocular lenses, aspheric designs are used to mimic the compensatory effect of the young crystalline lens [17,18].

Ocular surface geometry can be assessed by corneal topography [19], Scheimpflug imaging [20], or optical coherence tomography *in vivo* [21,22]. Shadow photography is used for crystalline lenses *in vitro* [23]. Profilometry is often used for plastic samples and artificial eyes [24,25].

All these techniques produce elevation maps that are affected by measurement noise. When fitting a noisy data set to a conic, two important issues may appear: First, the average radius and asphericity obtained from repeated measurements may be biased (i.e., when increasing the number of measurements the average value does not converge to the nominal value as a consequence of the nonlinear nature of conic curves) [26]. This problem is greatly alleviated when the fit is performed by minimizing the geometric distance between the data points and the curve [27], instead of other magnitudes [such as the residues of Eq. (1)] [28]. Another alternative for removing this bias from the data is to use an iterative procedure called renormalization that effectively weights each error according to its impact on the fitted parameters [26]. The second issue is that the values of R and Q obtained from fits to repeated noisy measurements of the same surface are strongly correlated, which has been reported in the area of image analysis [26]. This correlation has received much less attention than the bias.

In this study we show that this correlation is present in fits to measurements of human corneas collected with two different ocular topographers and also in data from artificial lenses collected with a profilometer, as well as in simulations. Furthermore, we note that it has an important effect when comparing different measurements, for example, in studies that address the differences of ocular biometry across populations, changes induced by a cor-

neal treatment, or changes in the crystalline lens with aging or accommodation. We find that the typical analysis in terms of separate changes in R and Q is not adequate due to the correlation, and propose what is to our knowledge a new statistical analysis that solves this problem.

2. MATERIALS AND METHODS

We studied the correlation between radius and asphericity in repeated measurements of corneal and intraocular lens surfaces fitted by conics. The analysis was performed on repeated measurements from three different instruments: Scheimpflug imaging topography, videokeratoscopy, and non-contact profilometry. We also performed computer simulations to explore the origin of the correlations. Measurements on patients followed the protocols approved by the Institutional Review Boards, and followed the tenets of the Declaration of Helsinki.

A. Scheimpflug Imaging Topography

We collected repeated measurements of the anterior and posterior corneal surfaces of three healthy eyes of three subjects with a Pentacam (Oculus, Wetzlar, Germany) Scheimpflug imaging topographer. This method provides quantitative elevation maps of both surfaces, sampled in a uniform square grid with a side of 100 μm (see Fig. 1, left) [9]. The instrument's software corrects the geometrical distortion of both corneal surfaces (due to the geometrical configuration of Scheimpflug cameras) and the optical distortion of the posterior surface (due to its imaging through the anterior corneal surface [14]). We collected 33 measurements of the right eye of Subject 1 (age 26), 23 measurements of the right eye of Subject 2 (age 25), and 35 measurements of the right eye of Subject 3 (age 37). All the measurements on each eye were taken consecutively in one single session, which took 45 min or less.

In addition to these data, we used data from a previous study [9] of 27 eyes of 14 patients before and after LASIK surgery, and 18 eyes of nine control subjects who did not undergo surgery, but that were measured at different time points. Each subject was measured in three or four experimental sessions on different days (over the first month post-surgery in patients and over 1 week for controls), and the measurements were repeated between three and six times per experimental session.

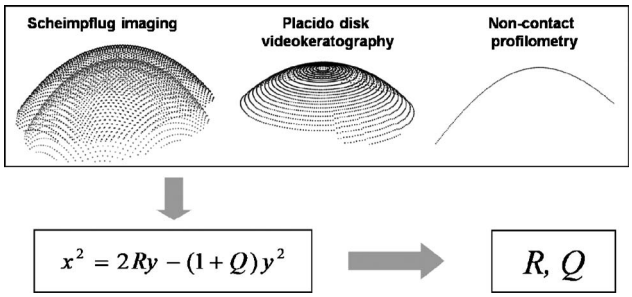

Fig. 1. Schematic diagram of the experimental methodology. Experimental data are obtained from real eyes with a Scheimpflug imaging topographer (left) and a Placido disk topographer (center), and from an intraocular lens with an optical profilometer (right). The data are exported to a computer, and fitted by ellipsoids or ellipses, described by given radius and asphericity.

B. Corneal Videokeratoscopy

We used an Atlas 990 (Carl Zeiss Meditec AG, Jena, Germany) topographer based on Placido disks to collect repeated measurements of the anterior corneal surface of eyes. We obtained 55 repeated measurements on Subject 1 and 20 measurements on Subject 2 (from the group of subjects described above). Each session took less than 2 h. The videokeratoscope provides a three-dimensional (3D) elevation map sampled in concentric circles around the corneal apex (see Fig. 1, center).

C. Lens Profilometry

In vivo corneal measurements are subject to variability in the sample and also to uncertainty in centration and alignment. We also used a microscopy-based non-contact optical profilometer (Plμ 2300, Sensofar, Barcelona, Spain) [29] to obtain repeated profilometric measurements of an aspheric intraocular lens (Alcon Acrysoft IQ, power 22 D, nominal $R=20$ mm, $Q=-33.23$) [30]. The instrument was programmed to take 36 two-dimensional (2D) profiles at identical exact conditions (within less than 140 min), using the confocal mode of the instrument, as described in [24]. Each profile extends about 5.5 mm, consisting of 1658 data points equi-spaced in the horizontal direction. The accuracy in the vertical direction is within 0.1 μm.

D. Simulations

We generated data sets following ideal rotationally symmetric ellipsoids, with the same sampling as the one used by Pentacam (grid of 100 μm squares). We also run simulations for 2D data. In this case we generated ellipses with the data points 100 μm apart. We added Gaussian noise along the apical direction (z-axis in the 3D data, y-axis in the 2D data) at each point, with a 10 μm standard deviation. The procedure was repeated 1000 times.

E. Fitting Procedures

All elevation maps were exported from the instruments and analyzed in Matlab (The Mathworks, Natick, MA, USA). For the corneal surfaces and simulations, we fitted the central 6 mm (diameter) of the elevation maps to quadrics [31], whose general equation is

$$\frac{x^2}{\alpha}+\frac{y^2}{\beta}+\frac{z^2}{\gamma}=1. \tag{2}$$

Rotationally symmetric quadrics have the restriction $\alpha=\beta$. When fitting corneal surfaces, we found that in all cases the best fit corresponded to an ellipsoid, i.e., α, β, and γ were positive. Radii and asphericities of the two main meridians are calculated as $R_x=\alpha/\sqrt{\gamma}$, $R_y=\beta/\sqrt{\gamma}$, $Q_x=\alpha/\gamma-1$, and $Q_y=\beta/\gamma-1$. In all cases, we allowed free translation in space of the fitting surface, but no rotation.

The profiles of the intraocular lens were fitted by conics [Eq. (1)]. In this case we allowed both free translation and rotation of the fitting curve, because we found that the

profiles were tilted. We fitted the entire profiles, which have a length of ~5.5 mm and are centered approximately at the apex.

The fitting was performed by minimizing the mean squared error along the z-axis for 3D measurements and along the y-axis for 2D measurements, using routines written in Matlab. As initial conditions, we used the result of minimizing the squared residues of Eqs. (1) and (2) (for the 2D and 3D cases, respectively). This minimization may be done very fast through a matrix inversion but the results are strongly affected by a bias [26], and that is why we only used this method to generate the initial conditions.

F. Statistical Analysis

We compared the usual statistical analysis that treats separately R and Q with a multivariate analysis of the variance (MANOVA) that takes into account both variables at the same time. Separate analyses of the two variables were done with Student's t-test. We considered that there was a change in the surface if we found a statistically significant change in R or in Q. As the probability of false positives roughly doubles with respect to using two variables, we applied a Bonferroni correction ($p=0.025$ in each of the two t-tests).

The MANOVA tests whether two sets of multidimensional measurements are different. For multidimensional measurements we mean those that are characterized by more than one scalar, as is the case of measurements of the corneal geometry that is characterized by R and Q. Briefly, MANOVA finds the direction of the R-Q plane in which the separation between the two data sets is maximum, and then performs a one-dimensional test along that direction, correcting the p-value for the extra degree of freedom introduced by the search of the direction of best discrimination. We used the implementation of MANOVA that is available in Matlab's statistics toolbox (function manova1). We use $p=0.05$ as the threshold between significant and non-significant differences.

3. RESULTS

A. Experimental Measurements

Figure 2 shows the correlation plot (radius versus asphericity) for repeated measurements of three subjects, taken with Pentacam. The data consist of 3D topographies, fitted to quadrics [Eq. (2)]. Figure 2(a) shows the data for the anterior cornea, and Fig. 2(b) for the posterior cornea. For the six data sets of repeated measurements, radii and asphericities of the fits are strongly and significantly correlated, except for the posterior surface of Subject 2 ($p=0.07$, circles; nonetheless, when the data were fitted to non-rotationally symmetric ellipsoids, there was a significant correlation in the vertical meridian, $p=0.02$). Table 1 shows the correlation coefficients (r) and p-values (p) for these measurements, as well as the slopes of the correlations. These data correspond to fits to rotationally symmetric ellipsoids, and the results hold (some of them with improved correlations) for non-rotationally symmetric ellipsoids.

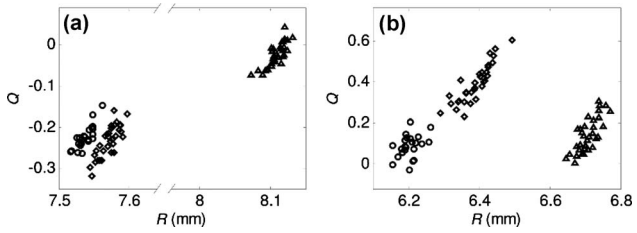

Fig. 2. Correlation between radius and asphericity when Pentacam data from repeated measurements are fitted to ellipsoids. (a) Data of anterior corneal surface. (b) Data of posterior corneal surface. Diamonds: Subject 1. Circles: Subject 2. Triangles: Subject 3.

In order to find the degree of correlation in a broader set of conditions, we analyzed a data set of repeated Pentacam measurements on patients before and after LASIK, at different time points, taken by three different operators in a clinical setting, and measurements of non-operated control subjects taken in a laboratory setting. This data set consists of measurements from different subjects obtained on different days (three to six measurements per day). Each data set is centered at its own mean value, which differs across subjects. As we are interested in comparing dispersion of the values, we subtracted the average values of radius and asphericity for each subject and session from all the measurements of the session. Figure 3(a) shows the correlation between the dispersion in R and Q of the anterior corneal surface, for all patients pre- and post-LASIK, and for all controls. Figure 3(b) shows the results for the posterior surface on the same eyes. The correlations are very strong ($r=0.93$ and $p<10^{-15}$ for the anterior surface, $r=0.77$ and $p<10^{-15}$ for the posterior), especially considering the heterogeneity of this set of measurements.

Figure 4 shows the correlation between R and Q from fits to the Placido videokeratoscopy data for Subject 1 [Fig. 4(a)] and Subject 2 [Fig. 4(b)]. As data are affected by the shadows and occlusions by the eyelashes and eyelids in the upper quarter of the topography, data in the horizontal meridian are more reliable than those of the vertical meridian, and only the radii and asphericities for the horizontal meridian are depicted. The correlation in the horizontal direction is stronger than the corresponding correlations in the vertical direction or for rotationally symmetric fits (not shown), but all correlations except one are significant (Table 1). In general, the videokeratoscopy data show a lower correlation than the Scheimpflug imaging data.

Figure 5 shows the correlation between radius and asphericity of repeated measurements of the profile of an aspheric intraocular lens, obtained with the Plμ non-contact optical profilometer. In this case, the data consist of a 2D profile, fitted by conics. The correlation is also very high: $r=0.83$, $p=4\times10^{-10}$.

B. Simulations

We built a synthetic data set corresponding to a perfect ellipsoid with $R=8$ mm and $Q=0.3$. When no noise is added to the data, the fitting algorithm provides exactly the correct ellipsoid parameters. The noise added to the synthetic ellipsoids causes dispersion in the fitted parameters (Fig. 6), and the correlation arises ($r=0.95$, $p<10^{-15}$). Figure 6 also shows the histograms along the R and Q directions. We see that, in spite of minimizing the

Table 1. Correlations between Fitted Radii and Asphericities in the Experimental Data

			Subject 1	Subject 2	Subject 3	Multiple[a]	IOL[b]
Scheimpflug imaging	Anterior surface	r[c]	0.82	0.83	0.76	0.93	—
		p[d]	$5\cdot10^{-9}$	$8\cdot10^{-7}$	10^{-7}	$<10^{-15}$	—
		m (mm^{-1})[e]	2.3±0.5	2.1±0.6	2.1±0.6	2.85±0.03	—
		n[f]	33	23	35	717	—
	Posterior surface	r	0.88	0.38	0.76	0.77	—
		p	10^{-11}	0.07	10^{-7}	$<10^{-15}$	—
		m (mm^{-1})	1.9±0.3	0.8±0.7	2.2±0.6	1.71±0.09	
		n	33	23	35	717	—
Placido disk videokeratoscopy	Symmetrical	r	0.39	−0.44		—	—
		p	0.003	0.06	—	—	—
		m (mm^{-1})	0.9±0.3	−0.3±0.7			
		n	55	20	—	—	—
	Horizontal meridian	r	0.54	0.53	—	—	—
		p	$2\cdot10^{-5}$	0.016	—	—	—
		m (mm^{-1})	0.8±0.3	0.6±0.4			
		n	55	20	—	—	—
	Vertical meridian	r	0.28	0.48	—	—	—
		p	0.04	0.03	—	—	—
		m (mm^{-1})	0.4±0.3	0.5±0.4			
		n	55	20	—	—	—
Profilometer		r	—	—	—	—	0.83
		p	—	—	—	—	$4\cdot10^{-10}$
		m (mm^{-1})					7.4±1.5
		n	—	—	—	—	36

[a]Data from a group of LASIK patients and non-operated controls.

[b]Intraocular lens.

[c]Correlation coefficient.

[d]p-value for the correlation.

[e]Slope of the correlation (and 95% confidence interval).

[f]Number of measurements.

geometrical distance between data and fitted curves, there is a slight bias in the average values. However, this bias is much smaller than the one reported for other types of fitting procedures [26].

We have found that the slope of the correlation depends on the average values of R and Q. In particular, the slope increases approximately linearly with R, and to a much lesser extent with Q. Also, the slope depends highly on the diameter of the fitting area, roughly doubling from a fit within a 6–4 mm diameter. It may also depend on other factors such as the type of noise, different samplings of the elevation map (square grid, rings, etc.), or unequal variance for the noise in different regions of the topography (for example, topographers are typically more accurate in the center than in the periphery). With respect to the latter case (differences in the effect of noise across the corneal topography), we observed in simulations that a very important bias in the average parameters occurs when noise in the periphery was greater than in the center. We found that the average Q shifted from the nominal

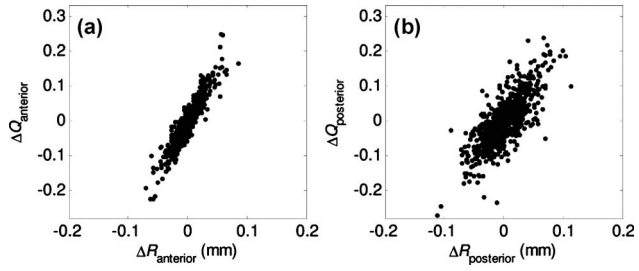

Fig. 3. Dispersion in fitted radius and asphericity from measurements obtained with Pentacam on different subjects (pre- and post-LASIK patients and controls) on different days (within 1 month, three to six consecutive measurements per session). (a) Anterior surface of the cornea. (b) Posterior surface of the cornea.

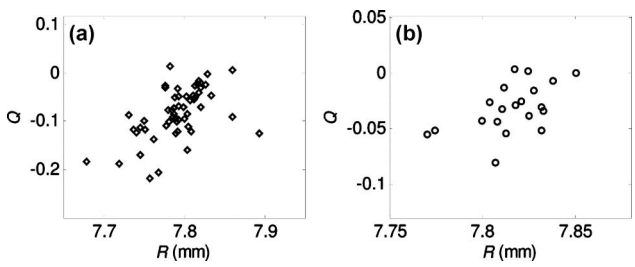

Fig. 4. Correlation between fitted radius and asphericity, for repeated measurements of the anterior corneal surface performed by Placido disk videokeratoscopy. (a) Subject 1. (b) Subject 2. Data are fitted to non-rotationally symmetric ellipsoids. The plotted data are for the horizontal meridian.

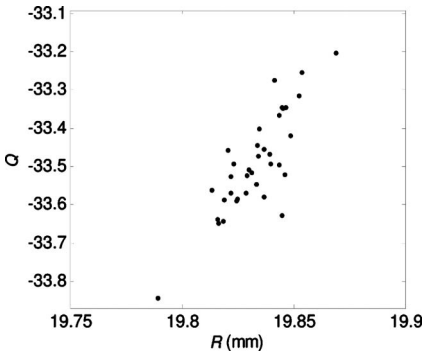

Fig. 5. Correlation between fitted radii and asphericities for repeated measurements on an aspheric intraocular lens, performed with a non-contact profilometer. Data are fitted by conics. This example corresponds to aspherical intraocular lens with a very high asphericity and very different geometry from that of normal eyes, and therefore the graph has been plotted with a different aspect ratio than Figs. 2–4.

0.3 to 0.9 and R shifted from the nominal 8 to 8.15 mm, for the 10 μm standard deviation in the central 3 mm and 20 μm standard deviation in the remaining area up to 6 mm diameter. A further study of these factors is necessary to characterize the correlation, but would be very instrument-specific, and falls beyond the scope of this paper.

We compared the slopes obtained by our simulations with the experimental results, by running simulations with the average experimental radii and asphericities and the same fitting region (central 6 mm diameter) and the noise values reported in the methods. We found for the simulated data slopes of 3 mm^{-1} for the anterior surface and of 2.5 mm^{-1} for posterior corneal surfaces, only slightly higher than the slopes found for the experimental data set (reported in Table 1). On the other hand simulations based on the average experimental radius and asphericities from fits of 2D profilometric data on intraocular lenses showed a slope of 7.1 mm^{-1}. In this case the slope of simulations falls within the confidence interval of the experimental result (see Table 1).

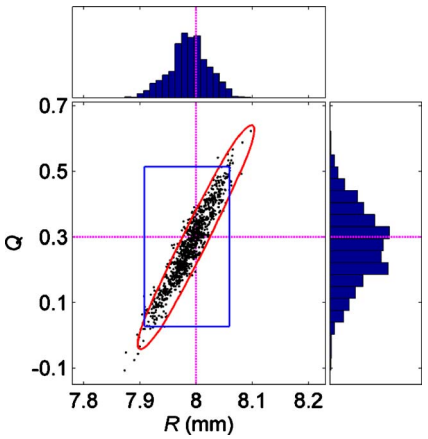

Fig. 6. (Color online) Results of the simulations for an ideal rotationally symmetric ellipsoid with $R=8$ mm and $Q=0.3$, and added Gaussian noise of 10 μm standard deviation. The central box shows the fitted parameters of 1000 fits, and the histograms show the dispersion in radius (top) and asphericity (right). The dashed lines indicate the nominal values. The elliptical contour limits the region where the mean squared error with respect to the nominal ellipsoid is lower than 0.5 μm (see Fig. 7). The rectangular contour limits the region of 95% confidence intervals in R and Q.

C. The Origin of the Correlation

The ellipsoids whose parameters lie along the line of correlation are very similar within the fitting region. To illustrate this, we built synthetic data sets of ellipsoids with radii ranging from 7.7 to 8.3 mm and asphericities ranging from −0.2 to 0.7 (no noise was added). Figure 7 shows the mean squared error between each of these ellipsoids and the one with $R=8$ mm and $Q=0.3$ (aligning them so that the mean squared error was minimum, and for a region of 6 mm of diameter around the apex). The region with the lowest difference is tilted in the R-Q plane. Furthermore, this region closely matches the parameters obtained by fitting noisy ellipsoids of $R=8$ mm and $Q=0.3$ (elliptic contour in Fig. 6). We conclude that the experimental noise produces a dispersion of the fitted parameters, with preference for ellipsoids that are statistically more similar to the nominal one. As the parameters of these similar ellipsoids are located along a diagonal in the R-Q space, the fitted data are correlated. We repeated the same calculation of the mean squared error using ellipses instead of ellipsoids, with similar results, indicating that the largest part of the effect is intrinsic to the geometry of ellipses, and not due to factors of the 3D geometry.

D. Consequences in the Statistical Analysis

In most literature in visual optics addressing corneal or crystalline lens geometry, the confidence intervals for radius and asphericity are calculated separately to analyze the significance of changes across patients, conditions, or treatment. The separate confidence intervals for radius and asphericity limit a region in the Q-R plane shown by the rectangle in Fig. 6 (95% confidence). However the true 95% confidence region (region inside which the 95% of the randomly generated points fall) is actually very different from the rectangle as it is close to the elliptical contour in Fig. 6. Considering the confidence intervals estimated by considering R and Q separately (rectangle) instead of the true region (ellipse) can lead to false positives and false negatives. Points within the rectangle but outside the el-

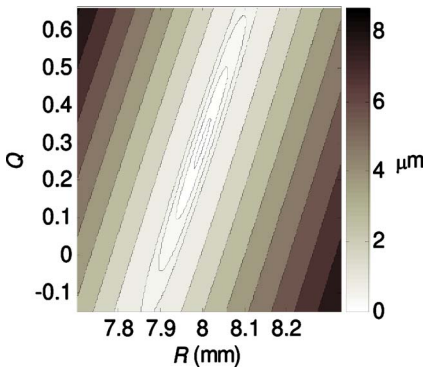

Fig. 7. (Color online) Mean squared error between an ellipsoid with $R=8$ mm and $Q=0.3$ and ellipsoids with the radii and asphericities specified in the axes. Contours have been plotted for mean squared errors at 0.2 μm steps between 0.1 and 0.7 μm and at 1 μm steps between 1 and 8 μm.

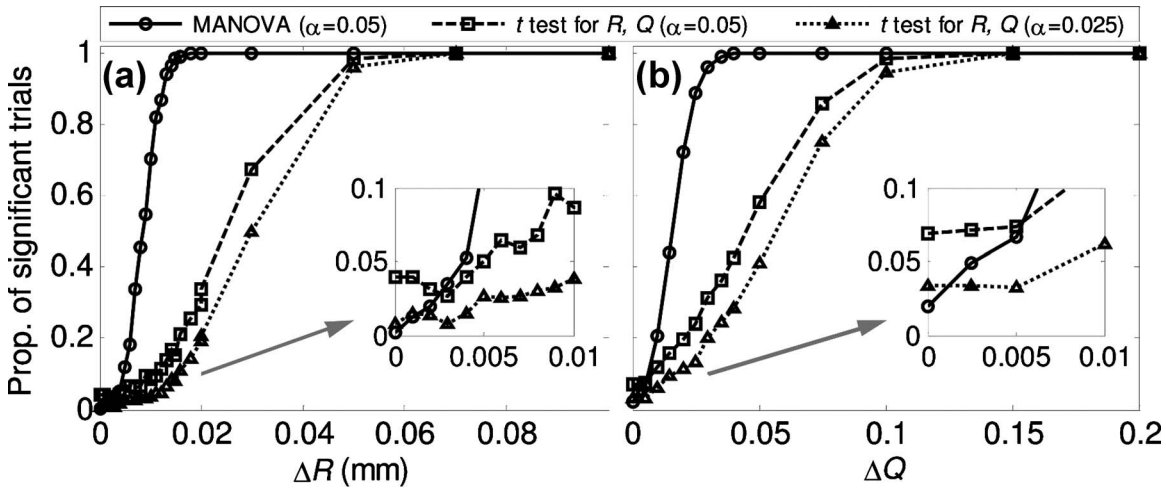

Fig. 8. Proportion of simulated experiments where a significant difference was detected between a reference ellipsoid with $R=8$ mm and $Q=0.3$ and a test ellipsoid with (a) $R=8+\Delta R$ mm and $Q=0.3$ or (b) $R=8$ mm and $Q=0.3+\Delta Q$. Each experiment compares five fits to the reference ellipsoid and five fits to the test one, simulating two sets of five repeated noisy measurements (10 μm standard deviation at each point of the ellipsoid). For each amount of change of R or Q, we simulated 1000 experiments, and the proportion of detected significant differences is plotted. Circles: Proportion of trials where MANOVA identified a significant change. Squares: Proportion of trials where the Student's t-test identified a significant change, either in radius or in asphericity. Triangles: Same as squares but applying the Bonferroni correction. Insets show a detail of the region near zero.

lipse will be erroneously identified as significantly different, decreasing the specificity of the test while points outside the ellipse but within the rectangle will be erroneously identified as not significantly different, decreasing the sensitivity of the test.

In order to overcome this problem one must use a multivariate statistical test, which takes into account the possible correlation between the two variables. We propose to use MANOVA.

Figure 8 compares the different sensitivities when using separated Student's t-tests for R and Q and when using MANOVA. In order to test the probability of detecting significant differences between corneal surfaces we simulated corneal topography measurements of pairs of corneal surfaces. One cornea had $R=8$ mm and $Q=0.3$ in all cases, while in the other R took values between 8 and 8.1 mm and $Q=0.3$ was constant [Fig. 8(a)], or Q took values between 0.3 and 0.5 and $R=8$ mm was constant [Fig. 8(b)]. To simulate realistic corneal topography measurements, Gaussian noise (with a standard deviation of 10 μm) was added to the ellipsoid. Each simulated experimental session consisted of five measurements per cornea. Each pair of series of five measurements was compared to estimate whether the two corneal surfaces were statistically different. Each experimental session was repeated 1000 times to obtain accurate probability estimates. Three statistical methods were tested: separate t-tests on R and Q, with and without the Bonferroni correction, and the MANOVA test proposed in this study. Figure 8 shows the probability that the two corneas are identified as significantly different, according to the three statistical methods. We found that MANOVA has higher sensitivity, being capable of detecting changes in R and Q about four times smaller than the separate tests. Also, MANOVA has a higher specificity, finding fewer false positives than the separate tests (Fig. 8, insets). The fact that the rate of false positives for MANOVA is lower than the expected 0.05 (because we set the threshold in $p=0.05$) is probably due to deviations of the data from ideal normal distributions. Both the Student's t-test and MANOVA share most assumptions about the data, including that of normally distributed data. However, MANOVA takes into account the possible correlation between the variables, which we have demonstrated to occur between R and Q of repeated measurements on the same surface.

Note that MANOVA does not use previous knowledge of the correlation between the two variables, and therefore it can be directly applied to any set of measurements. However, if the correlation specific to a given instrument is well known from a careful characterization, other statistical methods that make use of this previous knowledge can be implemented, increasing further the sensitivity and specificity of the tests.

4. DISCUSSION

The presence of strong correlations between radii and asphericities describing a surface obtained from multiple measurements has important implications in the detection of changes in conic surfaces. Certain combination of changes in the asphericity and radius along the correlation line can be interpreted as a change in the surface that does not really exist, while changes in radius and asphericity of the same magnitude but in the perpendicular direction can describe true significant changes in the surface. This is particularly important in physiological optics where conic surfaces are used to describe the surfaces of the ocular component. Studies of the geometry of crystalline lens reveal correlations between radius and asphericity [11] which may be overinterpreted as a particular feature of the lens, in association with development, growth, or aging. However, our results indicate that this is actually a consequence of the fit. Similarly, the impact of corneal treatments on the corneal geometry and optical quality is usually assessed in terms of changes in radius of curvature and asphericity [8,9]. Current efforts in refrac-

tive surgery aim at not inducing changes in the corneal asphericity to prevent the induction of spherical aberration. Statistical analysis of the significance of these changes should take into account the existing correlations between radius and asphericity in the statistical analysis of possible induced changes in asphericity.

5. CONCLUSIONS

There is an important degree of correlation between radius and asphericity, observed in repeated measurements of surface topography. The effect has been observed with different instruments (Scheimpflug imaging topographer, Placido disk videokeratoscope, and non-contact optical profilometer). This strong correlation holds across different measurement conditions and samples: anterior and posterior surfaces of the cornea *in vivo*, and intraocular lens *in vitro*. Simulations show that this correlation effect is produced even by subtle measurement noise or surface variability (as with the profilometer; Fig. 5). Measurement noise and surface variability will always be present experimentally, and we therefore can conclude that when fitting surface measurements to conics or conic-based surfaces the retrieved R and Q parameters will be usually correlated. It is clear from the examples and also from the simulations that when reporting the results of conic fittings, as those routinely used in ocular biometry, radius and asphericity cannot be treated separately: a correct description of the surface needs both parameters. We have proposed to use the statistical test MANOVA to study corneal changes. This test increases the sensitivity of the analysis, detecting changes about four times smaller than the separate analysis in R and Q.

ACKNOWLEDGMENTS

This research was funded by the Spanish Ministry of Science and Innovation Grants No. FIS2008-02065, and EURYI-05-102-ES (EURHORCs) to S. Marcos and predoctoral grant FPU (Beca para la Formación del Profesorado Universitario, ref. AP2006–01666) to A. Pérez-Escudero. The authors acknowledge technical assistance from Laura Remón, and fruitful discussions with Samuel Arba-Mosquera.

REFERENCES

1. P. Kiely, G. Smith, and L. Carney, "The mean shape of the human cornea," Opt. Acta **29**, 1027–1042 (1982).
2. A. Guirao and P. Artal, "Corneal wave aberration from videokeratography: accuracy and limitations of the procedure," J. Opt. Soc. Am. A **17**, 955–965 (2000).
3. W. Lotmar, "Theoretical eye model with aspheric surfaces," J. Opt. Soc. Am. A **61**, 1522–1529 (1971).
4. R. Mandell and R. St Helen, "Mathematical model of the corneal contour," Br. J. Physiol. Opt. **26**, 183–197 (1971).
5. L. Llorente, S. Barbero, D. Cano, C. Dorronsoro, and S. Marcos, "Myopic versus hyperopic eyes: axial length, corneal shape and optical aberrations," J. Vision **4**, 288–298 (2004).
6. P. M. Kiely, L. G. Carney, and G. Smith, "Diurnal variations of corneal topography and thickness," Am. J. Optom. Physiol. Opt. **59**, 976–982 (1982).
7. V. Sicam, M. Dubbelman, and R. G. L. van der Heijde, "Spherical aberration of the anterior and posterior surface of the human cornea," J. Opt. Soc. Am. A **23**, 544–549 (2006).
8. S. Marcos, D. Cano, and S. Barbero, "Increase of corneal asphericity after standard myopic LASIK surgery is not inherent to the Munnerlyn algorithm," J. Refract. Surg. **19**, 592–596 (2003).
9. A. Perez-Escudero, C. Dorronsoro, L. Sawides, L. Remon, J. Merayo-Lloves, and S. Marcos, "Minor influence of myopic maser *in situ* keratomileusis on the posterior corneal surface," Invest. Ophthalmol. Vis. Sci. **50**, 4146–4154 (2009).
10. F. Manns, A. Ho, J. M. Parel, and W. Culbertson, "Ablation profiles for wavefront-guided correction of myopia and primary spherical aberration," J. Cataract Refractive Surg. **28**, 766–774 (2002).
11. F. Manns, V. Fernandez, S. Zipper, S. Sandadi, M. Hamaoui, A. Ho, and J. M. Parel, "Radius of curvature and asphericity of the anterior and posterior surface of human cadaver crystalline lenses," Exp. Eye Res. **78**, 39–51 (2004).
12. C. E. Jones, D. A. Atchison, and J. M. Pope, "Changes in lens dimensions and refractive index with age and accommodation," Optom. Vision Sci. **84**, 990–995 (2007).
13. M. Dubbelman, G. L. Van der Heijde, and H. A. Weeber, "Change in shape of the aging human crystalline lens with accommodation," Vision Res. **45**, 117–132 (2005).
14. M. Dubbelman and V. Heijde, "The shape of the aging human lens: curvature, equivalent refractive index and the lens paradox," Vision Res. **41**, 1867–1877 (2001).
15. H. H. Dietze and M. J. Cox, "Correcting ocular spherical aberration with soft contact lenses," J. Opt. Soc. Am. A **21**, 473–485 (2004).
16. C. Dorronsoro, M. J. González, L. Llorente, and S. Marcos, "Optical and Visual quality with multifocal contact lenses," Invest. Ophthalmol. Vis. Sci. **48**, E-Abstract 5376 (2007).
17. J. Tabernero, P. Piers, A. Benito, M. Redondo, and P. Artal, "Predicting the optical performance of eyes implanted with IOLs to correct spherical aberration," Invest. Ophthalmol. Vis. Sci. **47**, 4651–4658 (2006).
18. S. Marcos, S. Barbero, and I. Jiménez-Alfaro, "Optical quality and depth-of-field of eyes implanted with spherical and aspheric intraocular lenses," J. Refract. Surg. **21**, 223–235 (2005).
19. J. Schwiegerling, J. Greivenkamp, and J. Miller, "Representation of videokeratoscopic height data with Zernike polynomials," J. Opt. Soc. Am. A **12**, 2105–2113 (1995).
20. M. Dubbelman, H. Weeber, R. Van Der Heijde, and H. Volker-Dieben, "Radius and asphericity of the posterior corneal surface determined by corrected Scheimpflug photography," Acta Ophthalmol. Scand. **80**, 379–383 (2002).
21. S. Radhakrishnan, A. Rollins, J. Roth, S. Yazdanfar, V. Westphal, D. Bardenstein, and J. Izatt, "Real-time optical coherence tomography of the anterior segment at 1310 nm," Arch. Ophthalmol. (Chicago) **119**, 1179–1185 (2001).
22. B. J. Kaluzy, J. J. Kaluzny, A. Szkulmowska, I. Gorczynska, M. Szkulmowski, T. Bajraszewski, M. Wojtkowski, and P. Targowski, "Spectral optical coherence tomography—A novel technique for cornea imaging," Cornea **25**, 960–965 (2006).
23. A. M. Rosen, D. B. Denharn, V. Fernandez, D. Boria, A. Ho, F. Matins, J. M. Parel, and R. C. Augusteyn, "*In vitro* dimensions and curvatures of human lenses," Vision Res. **46**, 1002–1009 (2006).
24. C. Dorronsoro, L. Remon, J. Merayo-Lloves, and S. Marcos, "Experimental evaluation of optimized ablation patterns for laser refractive surgery," Opt. Express **17**, 15292–15307 (2009).
25. C. Dorronsoro, D. Cano, J. Merayo, and S. Marcos, "Experiments on PMMA models to predict the impact of corneal refractive surgery on corneal shape," Opt. Express **14**, 6142–6156 (2006).
26. K. Kanatani, "Statistical bias of conic fitting and renormalization," IEEE Trans. Pattern Anal. Mach. Intell. **16**, 320–326 (1994).
27. Y. Nakagawa and A. Rosenfeld, "A note on polygonal and elliptical approximation of mechanical parts," Pattern Recogn. **11**, 133–142 (1979).

28. A. W. Fitzgibbon and R. B. Fischer, "A buyer's guide to conic fitting," in *Proceedings of the British Machine Vision Conference* (1995), pp. 265–271.
29. R. Artigas, F. Laguarta, and C. Cadevall, "Dual-technology optical sensor head for 3D surface shape measurements on the micro- and nanoscales," Proc. SPIE **5457**, 166–174 (2004).
30. X. Hong, J. Xie, S. J. N. Van, D. Stanley, M. Karakelle, M. J. Simpson, X. Zhang, "Ophthalmic lens as intraocular lens comprises optic having anterior surface and posterior surface, where at least one of the surfaces has an aspherical base profile such that the optic exhibits specific negative spherical aberration," patent WO2006108005-A2, 12 October 2006.
31. R. Navarro, L. Gonzalez, and J. L. Hernandez, "Optics of the average normal cornea from general and canonical representations of its surface topography," J. Opt. Soc. Am. A **23**, 219–232 (2006).